# Explorations of a Series of Second Order Nonlinear Optical Materials Based on Monovalent Metal Gold(III) Iodates

Chao Huang,[†,‡] Chun-Li Hu,[†] Xiang Xu,[†] Bing-Ping Yang,[†] and Jiang-Gao Mao*,[†]

[†]State Key Laboratory of Structural Chemistry, Fujian Institute of Research on the Structure of Matter, Chinese Academy of Sciences, Fuzhou 350002, People's Republic of China

[‡]University of the Chinese Academy of Sciences, Beijing 100039, People's Republic of China

Ⓢ *Supporting Information*
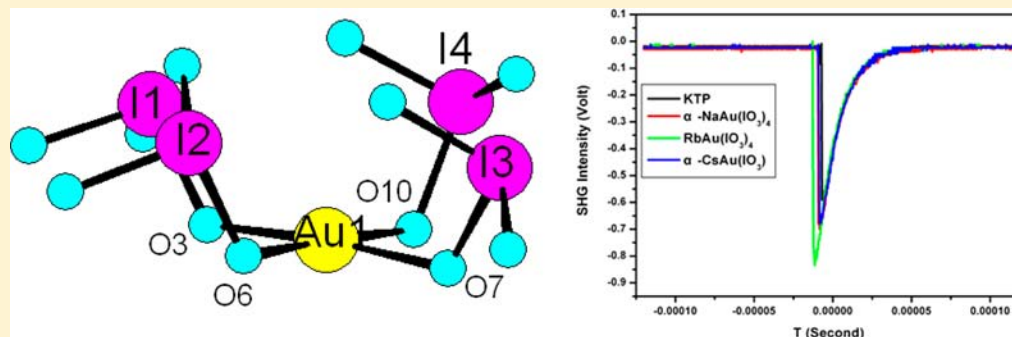
ABSTRACT: The syntheses, crystal structures, and characterizations of a series of monovalent metal gold(III) iodates, namely, α-NaAu(IO$_3$)$_4$, β-NaAu(IO$_3$)$_4$, RbAu(IO$_3$)$_4$, α-CsAu(IO$_3$)$_4$, β-CsAu(IO$_3$)$_4$, and AgAu(IO$_3$)$_4$ are reported. Their structures feature Au(IO$_3$)$_4^-$ anions that are separated by alkali metal ions or silver(I) ions. The Au(IO$_3$)$_4^-$ anions in the polar α-NaAu(IO$_3$)$_4$, RbAu(IO$_3$)$_4$, and α-CsAu(IO$_3$)$_4$ are polar with all four iodate groups being located only above (or below) the AuO$_4$ square plane (*cis*- configuration). α-NaAu(IO$_3$)$_4$, RbAu(IO$_3$)$_4$, and α-CsAu(IO$_3$)$_4$ display moderate strong Second-Hamonic Generation (SHG) responses of 1.17 ×, 1.33 ×, and 1.17 × KTP (KTiOPO$_4$), respectively, and all three materials are type-I phase-matchable. The Au(IO$_3$)$_4^-$ anions in centrysymmetric β-NaAu(IO$_3$)$_4$, β-CsAu(IO$_3$)$_4$, and AgAu(IO$_3$)$_4$ are nonpolar with the four iodate groups of the Au(IO$_3$)$_4^-$ anion being located both above and below the AuO$_4$ square plane (*trans*- configuration). IR and UV spectra, luminescent and ferroelectric properties have also been measured. Theoretical calculations of their optical properties based on density functional theory (DFT) methods were performed by using the CASTEP total-energy code.

■ INTRODUCTION

The search for new second-order nonlinear optical (NLO) materials is of current interest and great importance because of their applications in photonic technologies, such as laser frequency conversion, optical parameter oscillator (OPO), and signal communication.[1] Metal iodates are a very important class of second-order NLO materials because of their excellent overall properties such as high second-order NLO coefficients, wide transparent wavelength region, and relatively high stability.[2-4] Results of previous studies indicate the combination of the iodate anion with a cation containing lone pair electrons such as Bi^{3+} and Pb^{2+} is an effective route to design new second-order NLO materials with large Second-Hamonic Generation (SHG) responses,[5] as examplified by PbPt-(IO$_3$)$_6$(H$_2$O) (8 × KDP) and BiO(IO$_3$) (12.5 × KDP).[5a,c] Furthermore, various early transition-metal cations with a d^0 electronic configuration (e.g., Nb^{5+}, V^{5+}, Mo^{6+}) have been also introduced into the metal iodates to enhance their SHG responses by means of the additive polarizations from both types of asymmetric structural units originated from Second Order Jahn-Teller (SOJT) distortion,[6-8] which led to the discovery of a number

of new SHG materials including AMoO$_3$(IO$_3$) (A = Li, Rb, Cs),[6a] A$_2$Ti(IO$_3$)$_6$ (A = Li, Na),[7] BaNbO(IO$_3$)$_5$ (14 × KDP),[8a] NaVO$_2$(IO$_3$)$_2$(H$_2$O),[8c] and A(VO)$_2$(IO$_3$)$_3$O$_2$ (A = K, Rb, Cs, NH$_4$).[6b,8b] Their anionic structures usually feature various iso-lated clusters, one-dimensional (1D) chains and two-dimensional (2D) layers which are separated by charge balancing cations such as alkali, alkaline earth, lanthanide ions as well as other cations such as Ag$^+$, Tl$^+$, and Zn^{2+} ions. Recently it is reported that the iodates of transition metal ions with a square-planar geometry such as gold(III) and palladium(II) can also form NCS or polar structures and display good SHG properties, for example, BaPd(IO$_3$)$_4$ displays a moderate SHG efficiency of about 0.4 times that of KTP (KTiOPO$_4$).[9] It is noticed that such M(IO$_3$)$_4$ unit is usually anionic and requires charge balancing cations such as alkali or alkaline earth metal ions. Furthermore, the IO$_3$/M molar ratio has a very strong effect on the dimen-sionality of the anionic structures formed, for example, Pd(IO$_3$)$_2$, AgPd(IO$_3$)$_3$, and BaPd(IO$_3$)$_4$ feature a 2D Pd(IO$_3$)$_2$

Table 1. Summary of Crystal Data and Structural Refinements for the Six Compounds

compound	α-NaAu(IO$_3$)$_4$	β-NaAu(IO$_3$)$_4$	RbAu(IO$_3$)$_4$	α-CsAu(IO$_3$)$_4$	β-CsAu(IO$_3$)$_4$	AgAu(IO$_3$)$_4$
Fw	919.56	919.56	982.04	1029.48	1029.48	1004.44
crystal system	triclinic	monoclinic	monoclinic	monoclinic	triclinic	monoclinic
space group	$P1$ (No. 1)	$P2_1/c$ (No. 14)	$C2$ (No. 5)	$C2$ (No. 5)	$P\bar{1}$ (No. 2)	$P2_1/c$ (No. 14)
a/Å	5.4792(5)	11.0586(5)	13.538(11)	13.7753(16)	7.7104(4)	7.9892(3)
b/Å	7.0445(5)	4.40200(10)	5.474(4)	5.5886(3)	7.8890(4)	5.6513(2)
c/Å	8.1951(9)	12.5146(9)	8.394(6)	8.4817(7)	10.8936(6)	12.8052(5)
α/deg	105.837(8)	90	90	90	75.991(4)	90
β/deg	95.241(8)	116.644(4)	108.993(9)	108.940(13)	72.539(5)	107.468
γ/deg	110.269(8)	90	90	90	85.431(4)	90
V/Å^3	279.34(4)	919.56	588.1(8)	617.61(9)	613.28(6)	551.49(4)
Z	1	2	2	2	2	2
D_{calcd}/g·cm^{-3}	5.466	5.609	5.546	5.536	5.575	6.049
μ(Mo−Kα)/mm^{-1}	24.316	24.949	27.175	24.867	25.042	26.318
GOF on F^2	1.061	1.062	1.078	0.987	1.039	1.092
Flack factor	0.352(9)	none	0.125(17)	0.009(11)	none	none
R1, wR2 $(I > 2\sigma(I))^a$	0.0276, 0.0700	0.0212, 0.0465	0.0565, 0.1499	0.0305, 0.0674	0.0257, 0.0555	0.0252, 0.0609
R1, wR2 (all data)^a	0.0280, 0.0701	0.0248, 0.0486	0.0570, 0.1504	0.0315, 0.0679	0.0282, 0.0570	0.0261,0.0615

^{a}R1 = $\sum\|\|F_o\| - \|F_c\|\|/\sum\|F_o\|$, wR2 = $\{\sum[w(F_o^2 - F_c^2)^2]/\sum[w(F_o^2)^2]\}^{1/2}$.

layer, a 1D $[Pd(IO_3)_3]^-$ chain, and a 0D $[Pd(IO_3)_4]^{2-}$ unit, respectively.[9a] As an extension of our previous work, we started to explore the gold(III) iodates systematically; so far the only reported compound in this system is KAu(IO$_3$)$_4$,[9b] which crystallized in polar $P1$ space group, but unfortunately its SHG properties were not measured. Previous studies also revealed that the size of a countercation such as an alkali or alkaline earth metal ion has a great effect on the packing patterns of the polar anions, inducing the formation of a CS or NCS structure. For example, though all six compounds in the alkali-Ti^{4+}-iodate systems containing the same Ti(IO$_3$)$_6^{2-}$ unit, Li$_2$Ti(IO$_3$)$_6$ and Na$_2$Ti(IO$_3$)$_6$, are polar with strong SHG responses of 500 and 400 times that of α-SiO$_2$, respectively, whereas A$_2$Ti(IO$_3$)$_6$ (A = K, Rb, Cs, Tl) are structurally centrosymmetric (CS) and not SHG active.[7] Therefore it is very important to investigate and understand the effects of the sizes of the alkali metal ions on the crystal structures and SHG properties of alkali metal gold(III) iodates. Our systematic explorations of new SHG materials in the monovalent metal-Au-IO$_3$ systems led to the discovery of six new alkali metal or silver(I) gold(III) mixed metal iodates, namely, α-NaAu(IO$_3$)$_4$, β-NaAu(IO$_3$)$_4$, RbAu(IO$_3$)$_4$, α-CsAu-(IO$_3$)$_4$, β-CsAu(IO$_3$)$_4$, and AgAu(IO$_3$)$_4$. More interestingly α-NaAu(IO$_3$)$_4$, RbAu(IO$_3$)$_4$, and α-CsAu(IO$_3$)$_4$ display strong SHG responses of 1.17×, 1.33×, and 1.17 × KTP (KTiOPO$_4$), respectively. Furthermore all of them are type-I phase-matchable. Herein we report their syntheses, electron and crystal structures, luminescent, ferroelectric, and optical properties.

■ EXPERIMENTAL SECTION

Materials and Methods. All of the chemicals were obtained analytically pure from commercial sources and used without further purification. Na$_2$CO$_3$ (≥99.999%, Yixing No.2 Chemical Reagent Factory), Rb$_2$CO$_3$ (≥99.99%, Aladdin Chemistry Co. Ltd.), Cs$_2$CO$_3$ (≥99.99%, Aladdin Chemistry Co. Ltd.), Ag$_2$O (≥99%, Alfa Aesar), Au(OH)$_3$ (the content of gold ≥79%, Alfa Aesar), and I$_2$O$_5$ (≥99.99%, Shanghai Reagent Factory). Microprobe elemental analyses were performed on a field emission scanning electron microscope (FESEM, JSM6700F) equipped with an energy-dispersive X-ray spectroscope (EDS, Oxford INCA). The X-ray powder diffraction data were collected on a Panalytical X'pert Pro MPD diffractometer using graphite-monochromated Cu−Kα radiation in the 2θ range of 5−65° with a

step size of 0.02°. Thermogravimetric Analysis (TGA) and Differential Scanning Calorimetry (DSC) studies were all carried out with a NETZSCH STA 449C instrument. The sample and reference (Al$_2$O$_3$) were enclosed in a platinum crucible and heated at a rate of 10 °C/min from room temperature to 1000 °C under a nitrogen atmosphere. The IR spectra were recorded on a Magna 750 FT-IR spectrometer as KBr pellets in the range of 4000−400 cm^{-1}. The UV−vis absorption and optical diffuse reflectance spectra were measured at room temperature with a PE Lambda 900UV−vis spectrophotometer in the range of 2500−200 nm. BaSO$_4$ plate was used as a standard (100% reflectance). The absorption spectra were calculated from reflectance spectrum using the Kubelka−Munk function: $\alpha/S = (1 - R)^2/2R$,[10] where α is the absorption coefficient, S is the scattering coefficient that is practically wavelength independent when the particle size is larger than 5 μm, and R is the reflectance. Photoluminescent analyses were performed on an EI920 fluorescence spectrometer. The measurements of SHG were carried out on the sieved powder samples by using the Kurtz and Perry method with a 2.05 μm Q-switch laser.[11] The SHG efficiency has been shown to depend strongly on the particle size, thus the samples of α-NaAu(IO$_3$)$_4$, RbAu(IO$_3$)$_4$, and α-CsAu(IO$_3$)$_4$ were ground and sieved into several distinct particle size ranges (44−53, 53−74, 74−105, 105−149, 149−210, 210−270, and 270−325 μm). The sieved KTiOPO$_4$ (KTP) or KH$_2$PO$_4$ (KDP) powders were used as reference materials to assume the effect.

The ferroelectric properties of α-NaAu(IO$_3$)$_4$, RbAu(IO$_3$)$_4$, and α-CsAu(IO$_3$)$_4$ were measured on an aixACCT TF Analyzer 2000 ferroelectric tester at room temperature. α-NaAu(IO$_3$)$_4$, RbAu(IO$_3$)$_4$, and α-CsAu(IO$_3$)$_4$ powder were pressed into pellets (7.2-mm-diameter and 0.4-mm-thick, 7.2-mm-diameter and 0.42-mm-thick, 7.0-mm-diameter and 0.54-mm-thick, respectively) at room temperature, and the conducting Ag-glue was applied on the both sides of the pellets for electrodes.

Preparations of α-NaAu(IO$_3$)$_4$, RbAu(IO$_3$)$_4$, α-CsAu(IO$_3$)$_4$, and AgAu(IO$_3$)$_4$. These four compounds were synthesized by a similar method. Their single crystals were synthesized by the hydrothermal reactions of a mixture of Na$_2$CO$_3$ (0.03 mmol, 3.2 mg) (or Rb$_2$CO$_3$ (6.9 mg), Cs$_2$CO$_3$ (9.8 mg)), Ag$_2$O (7 mg), Au(OH)$_3$ (0.05 mmol, 12.4 mg), I$_2$O$_5$ (4 mmol, 333.8 mg), and 1 mL of water sealed in an autoclave equipped with a Teflon linear (23 mL) at 200 °C for 4 days, and then cooled to 30 °C at 3 °C/h. The final reaction products were washed with water and then dried in air. Yellow brick-shaped crystals of α-NaAu(IO$_3$)$_4$, green brick-shaped crystals of RbAu(IO$_3$)$_4$, kelly brick-shaped crystals of α-CsAu(IO$_3$)$_4$, and green brick-shaped crystals of AgAu(IO$_3$)$_4$ were obtained as a single phase in a yield of about 85%, 80%, 80%, and 85%, respectively (based on Au). Their purity were confirmed by X-ray diffraction (XRD) studies (Supporting Information,

Table 2. Important Bond Lengths (Å) and Angles (deg) for the Six Compounds[a]

		α-NaAu(IO$_3$)$_4$	
Au(1)−O(6)	1.963(12)	Au(1)−O(3)	1.980(12)
Au(1)−O(10)	1.983(11)	Au(1)−O(7)	1.986(12)
I(1)−O(2)	1.811(13)	I(1)−O(1)	1.810(11)
I(1)−O(3)	1.855(12)	I(2)−O(4)	1.798(11)
I(2)−O(5)	1.812(12)	I(2)−O(6)	1.902(12)
I(3)−O(9)	1.801(13)	I(3)−O(8)	1.797(12)
I(3)−O(7)	1.875(11)	I(4)−O(11)	1.793(12)
I(4)−O(12)	1.804(11)	I(4)−O(10)	1.893(11)
		β-NaAu(IO$_3$)$_4$	
Au(1)−O(1)#1	2.001(3)	Au(1)−O(1)#2	2.001(3)
Au(1)−O(6)#3	2.008(3)	Au(1)−O(6)	2.008(3)
I(1)−O(3)	1.797(3)	I(1)−O(2)	1.808(3)
I(1)−O(1)	1.903(3)	I(2)−O(4)	1.783(3)
I(2)−O(5)	1.792(3)	I(2)−O(6)	1.906(3)
		RbAu(IO$_3$)$_4$	
Au(1)−O(6)#1	1.980(13)	Au(1)−O(6)	1.980(13)
Au(1)−O(1)#1	2.011(16)	Au(1)−O(1)	2.011(16)
I(1)−O(2)	1.760(15)	I(1)−O(3)	1.826(17)
I(1)−O(1)	1.93(2)	I(2)−O(4)	1.744(17)
I(2)−O(5)	1.777(18)	I(2)−O(6)	1.890(17)
		α-CsAu(IO$_3$)$_4$	
Au(1)−O(1)#1	1.968(8)	Au(1)−O(1)	1.968(8)
Au(1)−O(6)#1	1.983(9)	Au(1)−O(6)	1.983(9)
I(1)−O(2)	1.788(10)	I(1)−O(3)	1.792(10)
I(1)−O(1)	1.903(10)	I(2)−O(4)	1.778(10)
I(2)−O(5)	1.809(12)	I(2)−O(6)	1.893(11)
		β-CsAu(IO$_3$)$_4$	
Au(1)−O(1)	1.976(5)	Au(1)−O(6)	1.977(5)
Au(1)−O(10)	1.987(5)	Au(1)−O(7)	1.994(5)
I(1)−O(3)	1.796(5)	I(1)−O(2)	1.810(5)
I(1)−O(1)	1.901(5)	I(2)−O(4)	1.786(5)
I(2)−O(5)	1.794(5)	I(2)−O(6)	1.885(5)
I(3)−O(9)	1.791(6)	I(3)−O(8)	1.797(5)
I(3)−O(7)	1.918(5)	I(4)−O(12)	1.785(5)
I(4)−O(11)	1.804(5)	I(4)−O(10)	1.910(5)
		AgAu(IO$_3$)$_4$	
Au(1)−O(1)#1	1.977(4)	Au(1)−O(1)	1.977(4)
Au(1)−O(5)	1.982(4)	Au(1)−O(5)#1	1.982(4)
I(1)−O(2)	1.797(5)	I(1)−O(3)	1.807(5)
I(1)−O(1)	1.881(5)	I(2)−O(4)	1.773(5)
I(2)−O(6)	1.831(4)	I(2)−O(5)	1.899(4)

[a]Symmetry transformations used to generate equivalent atoms: For β-NaAu(IO$_3$)$_4$: #1 x, $-y+3/2$, $z+1/2$; #2 $-x$, $y-1/2$, $-z+1/2$; #3 $-x$, $-y+1$, $-z+1$. For RbAu(IO$_3$)$_4$: #1 $-x$, y, $-z+1$. For α-CsAu(IO$_3$)$_4$: #1 $-x+2$, y, $-z+1$. For AgAu(IO$_3$)$_4$: #1 $-x+1$,$-y$,$-z+1$.

Figure S1). For the synthesis of RbAu(IO$_3$)$_4$, a very small amount of gold particles was also formed, and its XRD powder pattern revealed a diffraction peak at $2\theta = 38°$. The energy-dispersive spectrometry (EDS) elemental analyses on several single crystals for each compound gave average molar ratios of A (A = Na, Rb, Cs, Ag): Au: I of 1.2: 1: 3.2, 0.9: 1: 2.7, 0.9: 1: 3.4, and 0.9: 1: 3.2, respectively, for α-NaAu(IO$_3$)$_4$, RbAu(IO$_3$)$_4$, α-CsAu(IO$_3$)$_4$, and AgAu(IO$_3$)$_4$, which are in good agreement with those determined from single-crystal X-ray structural studies. IR data (KBr cm^{-1}): 765 (s), 741 (s), 670 (m), 642 (m), 528 (w), 505 (w) for α-NaAu(IO$_3$)$_4$; 773 (s), 668 (m), 621 (m), 523 (w), 501 (w) for RbAu(IO$_3$)$_4$; 821 (m), 780 (s), 753 (s), 688 (m), 642 (s), 517 (w), 487 (w) for α-CsAu(IO$_3$)$_4$; 833 (w), 756 (s), 695 (m), 672 (m), 641 (s), 502 (w) for AgAu(IO$_3$)$_4$ (Supporting Information, Figure S2).

Preparations of β-NaAu(IO$_3$)$_4$ and β-CsAu(IO$_3$)$_4$. These two compounds were synthesized by a similar method. Their single crystals
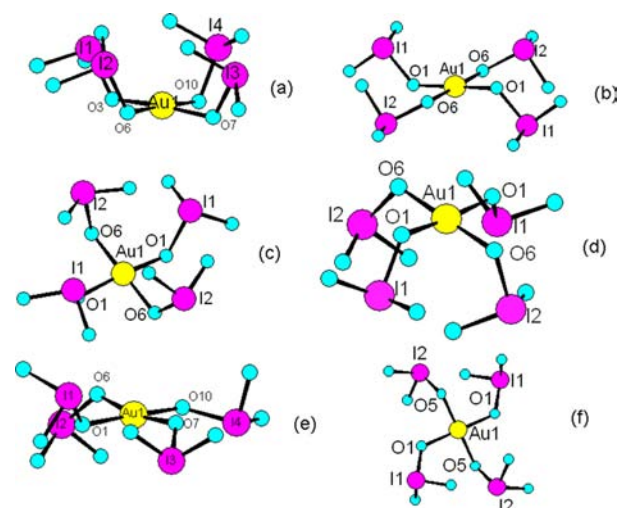
Figure 1. View of the $[\text{Au(IO}_3)_4]^-$ anions in α-NaAu(IO$_3$)$_4$ (a), β-NaAu(IO$_3$)$_4$ (b), RbAu(IO$_3$)$_4$ (c), α-CsAu(IO$_3$)$_4$ (d), β-CsAu(IO$_3$)$_4$ (e), and AgAu(IO$_3$)$_4$ (f).

were synthesized by the hydrothermal reactions of a mixture of Na$_2$CO$_3$ (0.03 mmol, 3.2 mg) or Cs$_2$CO$_3$ (0.03 mmol, 9.8 mg), Au(OH)$_3$ (0.05 mmol, 12.4 mg), I$_2$O$_5$ (4 mmol, 333.8 mg), and 1 mL of water sealed in an autoclave equipped with a Teflon linear (10 mL) at 190 °C for 4 days, and then cooled to 30 °C at 3 °C/h. The final reaction products were washed with water and then dried in air. Orange brick-shaped crystals of β-NaAu(IO$_3$)$_4$ and red brick-shaped crystals of β-CsAu(IO$_3$)$_4$ were collected in yield of about 85% and 80%, respectively, based on Au as single phases. Their purity were confirmed by XRD studies (Supporting Information, Figure S1). The energy-dispersive spectrometry (EDS) elemental analyses on several single crystals for each compound gave average molar ratio of A (A = Na, Cs): Au: I of 1.1: 1: 3.3 and 0.9: 1: 3.2, respectively for β-NaAu(IO$_3$)$_4$ and β-CsAu(IO$_3$)$_4$, which are in good agreement with those determined from single-crystal X-ray structural studies. IR data (KBr cm^{-1}): 799 (m), 757 (s), 629 (m), 553 (w), 507 (w) for β-NaAu(IO$_3$)$_4$; 832 (m), 800 (s), 769 (s), 741 (s), 701 (m), 655 (s), 533 (w), 492 (w), 460 (w) for β-CsAu(IO$_3$)$_4$ (Supporting Information, Figure S2).

Single-Crystal Structure Determination. Single-crystal XRD data for all of six compounds were collected on an Agilent Technologies SuperNova Dual Wavelength CCD diffractometer equipped with a graphite-monochromated Mo−Kα radiation ($\lambda = 0.71073$ Å) at 293 K. The data sets were corrected for Lorentz and polarization factors as well as for absorption by the SADABS program. All of the six structures were solved by the direct method and refined by full-matrix least-squares fitting on F^2 by SHELX-97.[12] The Flack factors for α-NaAu(IO$_3$)$_4$, RbAu(IO$_3$)$_4$, and α-CsAu(IO$_3$)$_4$ are refined to be 0.352(9), 0.126(17), and 0.009(11), indicating that there exists a small degree of racemic twinning for α-NaAu(IO$_3$)$_4$ and RbAu(IO$_3$)$_4$. The silver atom (Ag(1)) in AgAu(IO$_3$)$_4$ is disordered over two sites related by an inversion center with Ag···Ag distance of 1.470(3) Å; hence, its occupancy factor is reduced to 50%.

Crystallographic data and structural refinement for the compounds are summarized in Table 1. Important bond distances are listed in Table 2. More details on the crystallographic studies are given as Supporting Information.

Computational Details. Single crystal structural data of three polar compounds (α-NaAu(IO$_3$)$_4$, RbAu(IO$_3$)$_4$, and α-CsAu(IO$_3$)$_4$) were used for the theoretical calculations with the total-energy code CASTEP.[13] Band structures, density of states (DOS), and optical properties were calculated with density functional theory (DFT) using the Perdew−Burke−Ernzerhof (PBE) generalized gradient approximation.[14] The interactions between the ionic cores and the electrons were described by a norm-conserving pseudopotential.[15] The following orbital electrons were treated as valence electrons: Na-2s^{2}2p^{6}3s^1,
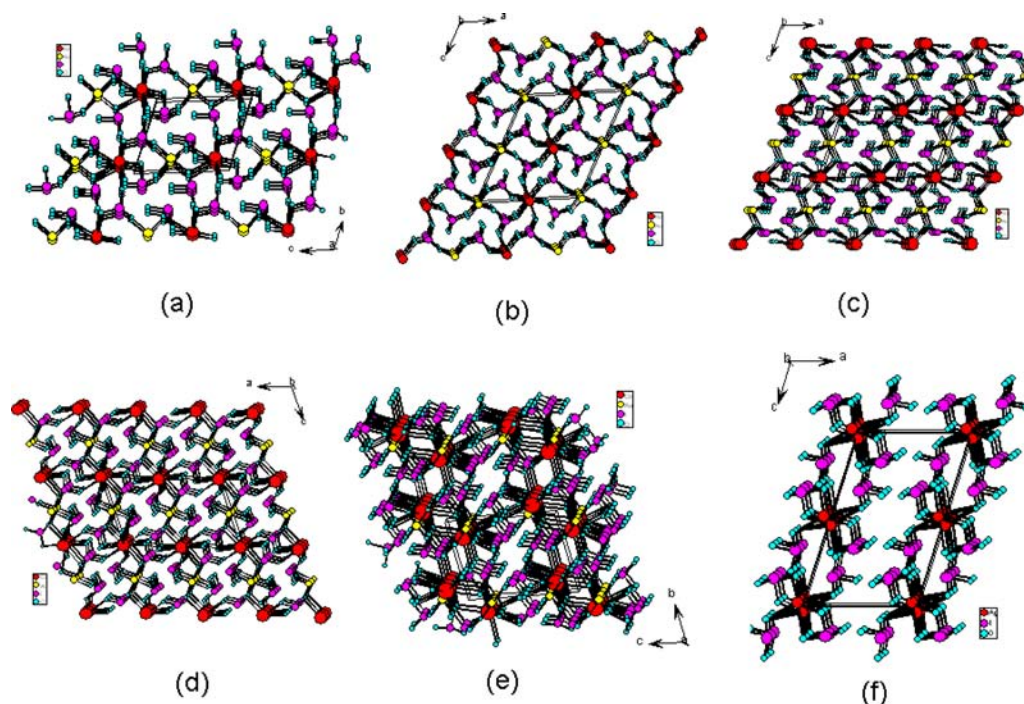
Figure 2. Views of the structures of α-NaAu(IO$_3$)$_4$ (a), β-NaAu(IO$_3$)$_4$ (b), RbAu(IO$_3$)$_4$ (c), α-CsAu(IO$_3$)$_4$ (d), β-CsAu(IO$_3$)$_4$ (e), and AgAu(IO$_3$)$_4$ (f).
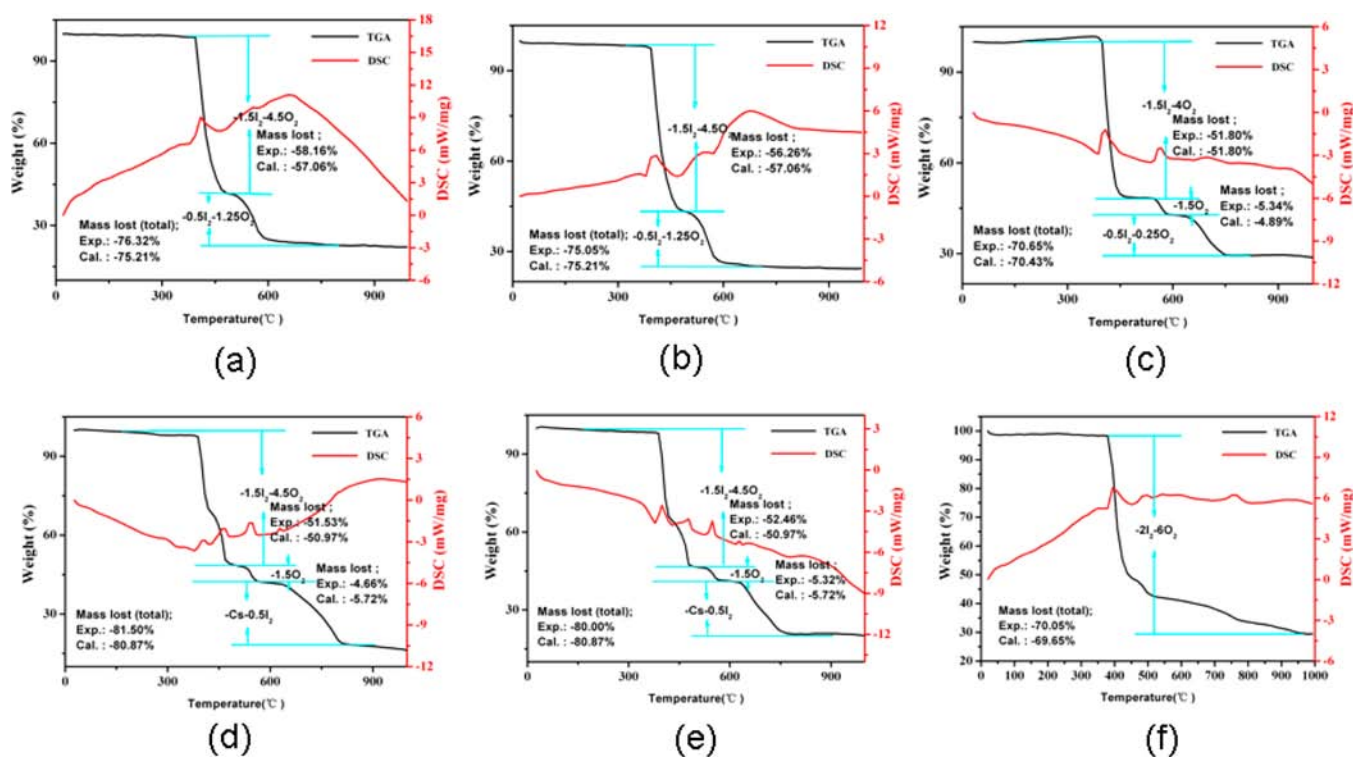
Figure 3. TGA and DTA curves for α-NaAu(IO$_3$)$_4$, β-NaAu(IO$_3$)$_4$, RbAu(IO$_3$)$_4$, α-CsAu(IO$_3$)$_4$, β-CsAu(IO$_3$)$_4$, and AgAu(IO$_3$)$_4$.

Rb-4s^{2}4p^{6}5s^1, Cs-5s^{2}5p^{6}6s^1, Au-5d^{10}6s^1, I-5s^{2}5p^5, and O-2s^{2}2p^4. The numbers of plane waves included in the basis sets were determined by a cutoff energy of 750 eV, and the numerical integration of the Brillouin zone was performed using Monkhorst−Pack k-point sampling of 5 × 4 × 3, 2 × 5 × 3, and 2 × 4 × 3, respectively for α-NaAu(IO$_3$)$_4$, RbAu(IO$_3$)$_4$, and α-CsAu(IO$_3$)$_4$. The other parameters and convergent criteria were the default values of the CASTEP code.

The calculations of linear optical properties were made in terms of the complex dielectric function $\varepsilon(\omega) = \varepsilon_1(\omega) + i\varepsilon_2(\omega)$. The imaginary part of the dielectric function ε_2 is given in the following equation.[16]

$$\varepsilon_2^{ij}(\omega) = \frac{8\pi^2\hbar^2 e^2}{m^2 V} \sum_k \sum_{cv} (f_c - f_v) \frac{p_{cv}^i(k)\, p_{vc}^j(k)}{E_{vc}^2}$$

$$\delta[E_c(k) - E_v(k) - \hbar\omega] \tag{1}$$
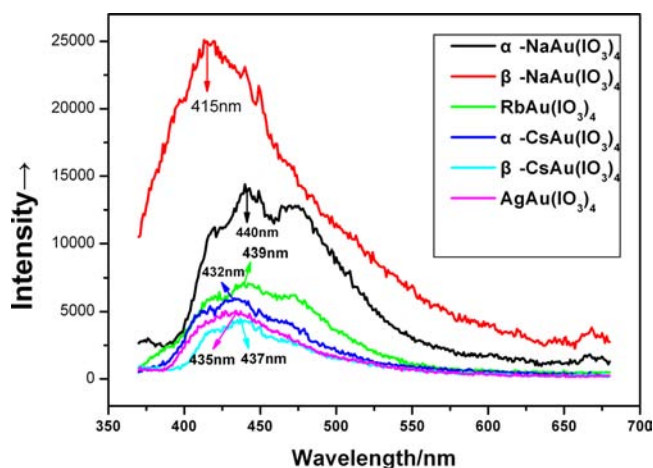
Figure 4. Solid State emission spectra of α-NaAu(IO$_3$)$_4$, β-NaAu-(IO$_3$)$_4$, RbAu(IO$_3$)$_4$, α-CsAu(IO$_3$)$_4$, β-CsAu(IO$_3$)$_4$, and AgAu(IO$_3$)$_4$ under λ_{ex} = 350 nm.

The f_c and f_v represent the Fermi distribution functions of the conduction and valence bands, respectively. The term $p_{cv}^i(k)$ denotes the momentum matrix element transition from the energy level "c" of the conduction band to the level "v" of the valence band at a certain k point in the Brillouin zones, and V is the volume of the unit cell. The m, e, and $\hbar$ are the electron mass, charge, and Planck's constant, respectively.

The second-order optical properties were calculated based on momentum-gauge formalism with the minimal-coupling interaction Hamiltonian and within the independent-particle approximation.[17] The imaginary part of the frequency-dependent second-order susceptibility $\chi^{(2)}(2\omega,\omega,\omega)$ is obtained from the electronic band structures by using the expressions already given elsewhere.[18] We then use the Kramers−Kronig relations, as required by causality, to obtain the real part

$$\chi'^{(2)}(-2\omega,\ \omega,\ \omega) = \frac{2}{\pi}P\int_0^\infty \mathrm{d}\omega'\frac{\omega'\chi''^{(2)}(2\omega',\ \omega',\ \omega')}{\omega'^2 - \omega^2} \qquad (2)$$

In the present study, the δ function in the expressions for $\chi^{(2)}(2\omega,\omega,\omega)^{18a-c}$ was approximated by a Gaussian function with Γ = 0.2 eV. Furthermore, to ensure that the real part calculated via Kramers−Kronig transformation (eq 2) is reliable, 120 and 240 empty bands were used in optical calculation for α-NaAu(IO$_3$)$_4$ and RbAu(IO$_3$)$_4$ (α-CsAu(IO$_3$)$_4$). In addition, because DFT-GGA fails to correctly predict the CB energies, the CB energy must be corrected by adding a scissor operator; in addition, the momentum matrix elements were also renormalized.[18a]

■ RESULTS AND DISCUSSION

A series of novel monovalent metal gold(III) iodates with square-planar AuO$_4$ units, namely, α-NaAu(IO$_3$)$_4$, β-NaAu(IO$_3$)$_4$, RbAu-(IO$_3$)$_4$, α-CsAu(IO$_3$)$_4$, β-CsAu(IO$_3$)$_4$, and AgAu(IO$_3$)$_4$, have been successfully synthesized through hydrothermal reactions. It should be noted that all six compounds were synthesized using
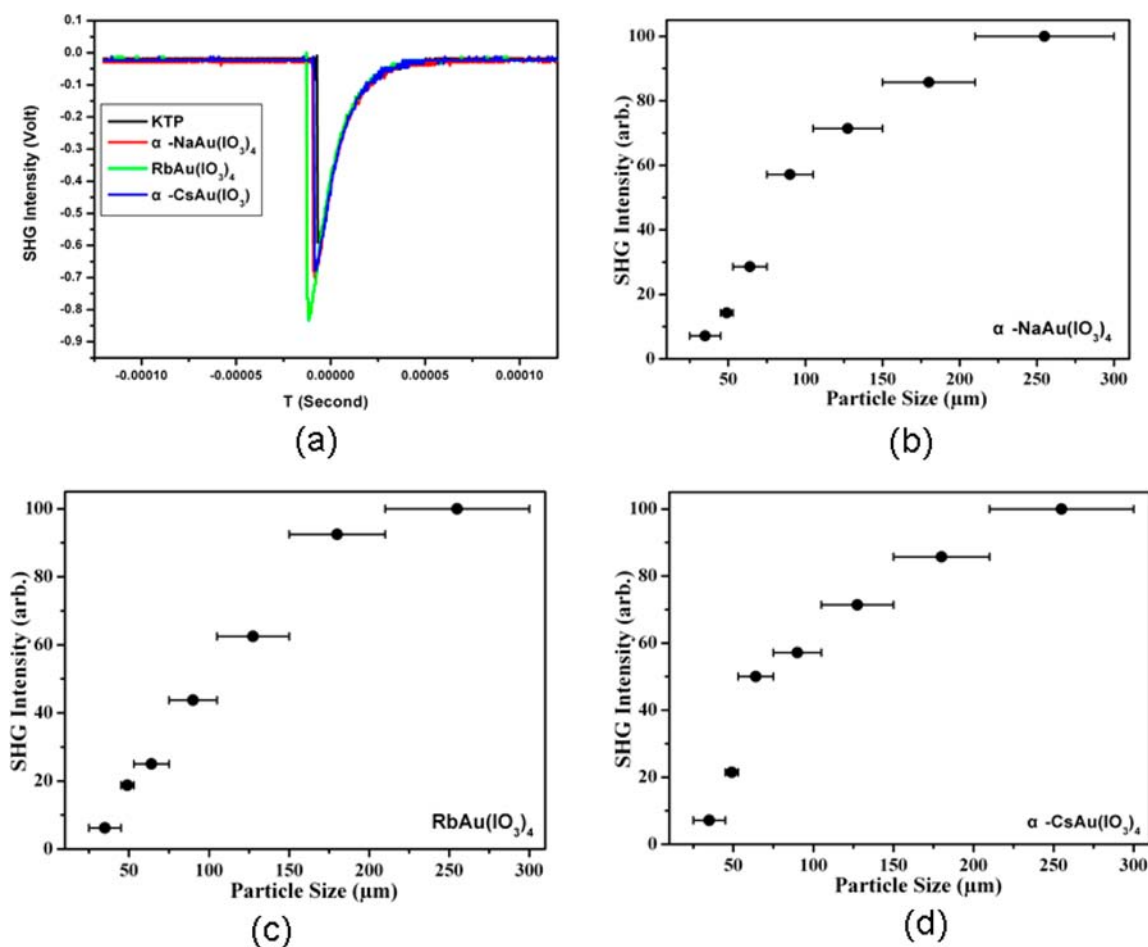
Figure 5. Oscilloscope traces of the SHG signals for the powders (270−325 μm) of KTP, α-NaAu(IO$_3$)$_4$, RbAu(IO$_3$)$_4$, and α-CsAu(IO$_3$)$_4$ (a), and phase-matching curves for α-NaAu(IO$_3$)$_4$ (b), RbAu(IO$_3$)$_4$ (c), and α-CsAu(IO$_3$)$_4$ (d). The curves drawn are to guide the eye and not a fit to the data.
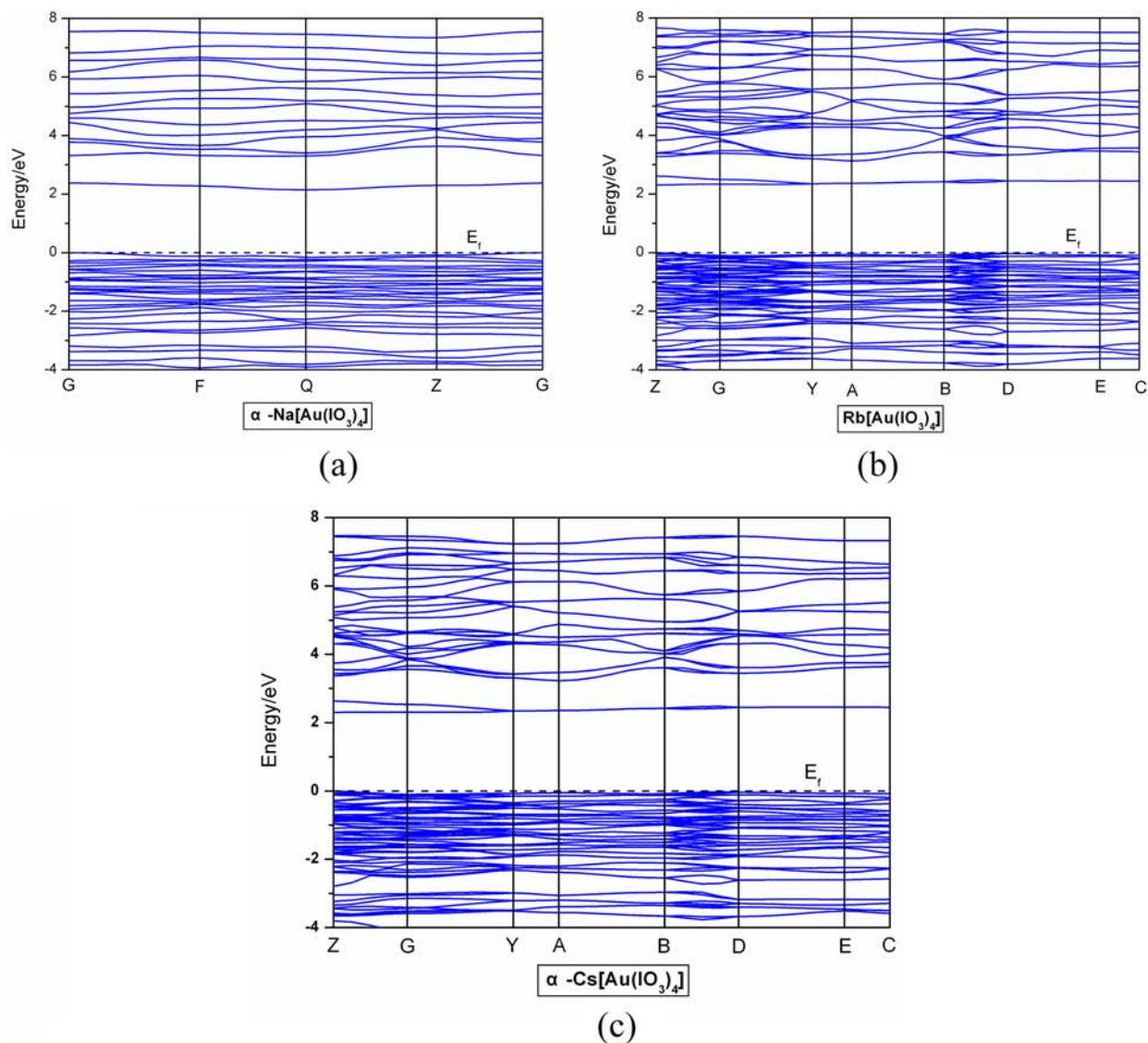
Figure 6. Band structures for the crystals α-NaAu(IO₃)₄ (a), RbAu(IO₃)₄ (b), and α-CsAu(IO₃)₄ (c) (the Fermi level is set at 0 eV).

the same molar ratios of A (A = Na, Rb, Cs, Ag): Au: I. α-NaAu(IO₃)₄, RbAu(IO₃)₄, α-CsAu(IO₃)₄, and AgAu(IO₃)₄ were synthesized at 200 °C whereas β-NaAu(IO₃)₄ and β-CsAu(IO₃)₄ were synthesized at a lower temperature of 190 °C but under a much higher pressure because of the much smaller volume of the Teflon linear used (10 mL versus 23 mL). It is found that β-form materials have slightly larger densities than their corresponding α-form ones. The amount of starting materials and water are the same for the syntheses of two pairs of α- and β-form materials. Hence, the reaction temperature and pressure have a strong effect on the structures of the materials formed.

Structural Descriptions. All of the six compounds feature Au(IO₃)₄⁻ anions that are separated by alkali metal ions or silver(I) ions; however, the geometries of the Au(IO₃)₄⁻ anions can be different, and the different packing patterns of these Au(IO₃)₄⁻ anions in their unit cells can lead to centrosymmetric (CS) or non-centrosymmetric (NCS) structures, which is also affected by the countercation and the preparation methods. α-NaAu(IO₃)₄ is isostructural with KAu(IO₃)₄ and crystallized in the polar space group P1.[9b] RbAu(IO₃)₄ and α-CsAu(IO₃)₄ are isostructural and crystallized in the polar

space group C2. β-NaAu(IO₃)₄, β-CsAu(IO₃)₄, and AgAu-(IO₃)₄ are centrosymmetric with space group P2₁/c, P1̄, and P2₁/c, respectively. The structures of the Au(IO₃)₄⁻ anions in the six compounds are shown in Figure 1. The gold(III) ions in all six compounds are in a square planar geometry formed by four oxygen atoms from four iodate groups. The Au—O distances are in the ranges of 1.963(12)−1.986(12) Å, 2.001(3)−2.008(3) Å, 1.978(13)−2.011(16) Å, 1.968(8)−1.983(9) Å, 1.976(5)−1.994(5) Å, 1.977(4)−1.982(4) Å, respectively for α-NaAu(IO₃)₄, β-NaAu(IO₃)₄, RbAu(IO₃)₄, α-CsAu(IO₃)₄, β-CsAu(IO₃)₄, and AgAu(IO₃)₄. All of I⁵⁺ cations adopt a ψ-IO₃ trigonal pyradimal geometry with the pyramidal site occupied by the lone pair electrons. The I—O distances are in the ranges of 1.793(12)−1.902(12) Å, 1.792(3)−1.906(3) Å, 1.764(15)−1.93(2) Å, 1.778(10)−1.903(10) Å, 1.786(5)−1.918(5) Å, 1.773(5)−1.899(4) Å, respectively, for α-NaAu(IO₃)₄, β-NaAu(IO₃)₄, RbAu(IO₃)₄, α-CsAu(IO₃)₄, β-CsAu(IO₃)₄, and AgAu(IO₃)₄. These I—O and Au—O distances are close to those reported in K[Au(IO₃)₄] and other related compounds.[9,19] It is noticed that all four iodate groups are located at the same side of the AuO₄ square plane in polar α-NaAu(IO₃)₄, RbAu(IO₃)₄, and α-CsAu(IO₃)₄. The distances of the four I⁵⁺ ions from the
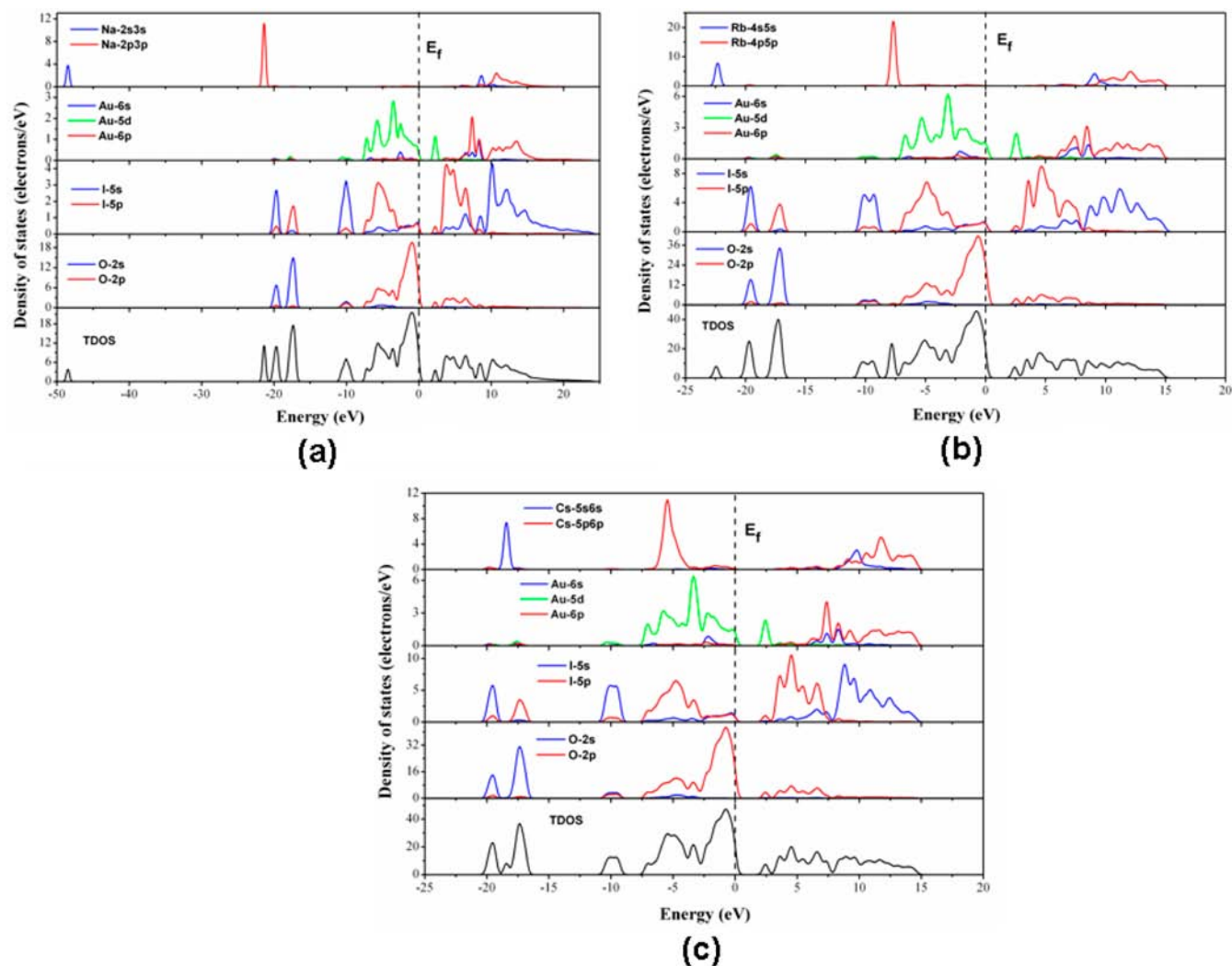
Figure 7. Total density of states and partial density of states of α-NaAu(IO$_3$)$_4$ (a), RbAu(IO$_3$)$_4$ (b), and α-CsAu(IO$_3$)$_4$ (c) (the Fermi level is set at 0 eV).

Table 3. Angles between the Crystallography Axes[a] and the Principal Dielectric Axes[b] in the Triclinic Crystal α-NaAu(IO$_3$)$_4$

| ∠	a-O-x	b-O-x	c-O-x	a-O-y	b-O-y	c-O-y	a-O-z	b-O-z	c-O-z
angle (deg)	2.93	112.29	96.57	87.42	28.70	91.56	88.61	107.13	6.75

[a] a, b, and c. [b] x, y, and z.

AuO$_4$ plane are 1.4528−1.7229 Å, 1.4921−1.7622 Å, 1.4423−1.7239 Å, respectively for α-NaAu(IO$_3$)$_4$, RbAu(IO$_3$)$_4$, and α-CsAu(IO$_3$)$_4$. These [Au(IO$_3$)$_4$]$^-$ anions are polar and have net polarizations along the axial direction which is perpendicular to the AuO$_4$ plane. For the three compounds with CS structure, the four iodate groups of the [Au(IO$_3$)$_4$]$^-$ anion are located at both sides of the AuO$_4$ plane; hence these [Au(IO$_3$)$_4$]$^-$ anions have no (for β-NaAu(IO$_3$)$_4$ and AgAu(IO$_3$)$_4$) or very small (β-CsAu(IO$_3$)$_4$) net dipole moments.

The above polar or nonpolar [Au(IO$_3$)$_4$]$^-$ anions are interconnected by alkali metal ions or silver(I) ions into layered (for Ag compound) or 3D network structures (for the remaining five compounds) (Figure 2). The sodium(I) ion in α-NaAu(IO$_3$)$_4$ is coordinated by eight oxygen atoms from eight iodate groups with Na−O distances in the range of 2.500(14)−3.000(15) Å whereas sodium(I) ion in β-NaAu(IO$_3$)$_4$ is octahedrally coordinated by six oxygen atoms from six iodate groups with Na−O distances in the range of 2.400(3)−2.416(3) Å (Supporting Information, Figure S3). The rubidium(I) ion in RbAu(IO$_3$)$_4$ is coordinated

by 12 oxygen atoms from 8 iodate groups with Rb−O distances in the range of 2.863(15)−3.438(17) Å. The cesium(I) ion in α-CsAu(IO$_3$)$_4$ is coordinated by 12 oxygen atoms from 8 iodate groups with Cs−O distances in the range of 2.966(9)−3.520(9) Å whereas cesium(I) ion in β-CsAu(IO$_3$)$_4$ is coordinated by 11 oxygen atoms from 8 iodate groups with Cs−O distances in the range of 3.040(5)−3.732(5) Å (Supporting Information, Figure S3). The silver(I) ion in AgAu(IO$_3$)$_4$ is coordinated by 5 oxygen atoms from four iodate groups with Ag−O distances in the range of 2.366(5)−2.582(7) Å. The polar [Au(IO$_3$)$_4$]$^-$ anions in α-NaAu(IO$_3$)$_4$, RbAu(IO$_3$)$_4$, and α-CsAu(IO$_3$)$_4$ are properly aligned to produce a large macroscale polarization, which is confirmed by the results of SHG measurements as will be discussed later.

Thermal Stability Studies. TGA studies indicate that α-NaAu(IO$_3$)$_4$, β-NaAu(IO$_3$)$_4$, RbAu(IO$_3$)$_4$, α-CsAu(IO$_3$)$_4$, β-CsAu(IO$_3$)$_4$, and AgAu(IO$_3$)$_4$ are all thermally stable up to about 380 °C. Then AgAu(IO$_3$)$_4$ displays one step of weight loss, and α-NaAu(IO$_3$)$_4$ and β-NaAu(IO$_3$)$_4$ display two steps of
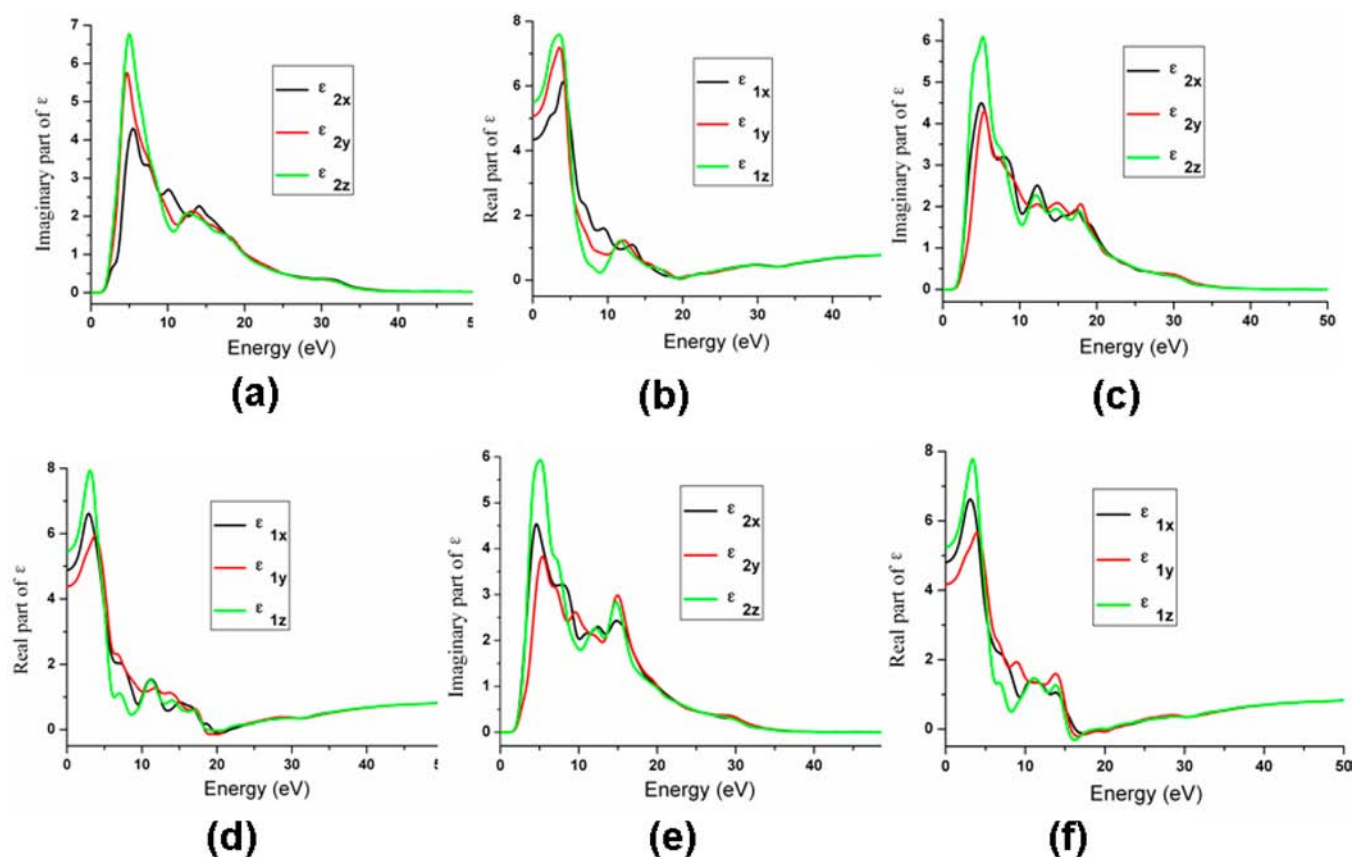
Figure 8. Calculated imaginary part and the real part of the dielectric function polarized along three dielectric axes directions for α-NaAu(IO$_3$)$_4$ (a and b), RbAu(IO$_3$)$_4$ (c and d), and α-CsAu(IO$_3$)$_4$ (e and f).

weight losses whereas the other three compounds each display three main steps of weight losses (Figure 3). For AgAu(IO$_3$)$_4$, the weight losses in the temperature ranges 380−1000 °C corresponds to the release of 2 I$_2$ and 6 O$_2$ per formula unit. The total weight loss at 1000 °C is 70.05%. For α-NaAu(IO$_3$)$_4$ and β-NaAu(IO$_3$)$_4$, the weight loss in the temperature range of 380−480 °C corresponds to the release of 1.5 I$_2$ and 4.5 O$_2$ per formula unit. The residuals at 480 °C are expected to be NaIO$_3$ and Au, the observed weight losses of 58.16% and 56.26%, respectively, for α-NaAu(IO$_3$)$_4$ and β-NaAu(IO$_3$)$_4$ are close to the calculated values 57.06%. The second weight losses in the temperature range of 480−600 °C correspond to further decomposition of the compounds. The total weight losses at 1000 °C are 76.32% and 75.05% respectively for α-NaAu(IO$_3$)$_4$ and β-NaAu(IO$_3$)$_4$, which are close to the calculated value of 75.21% if the final residuals at 1000 °C are assumed to be a mixture of Na$_2$O and Au.

For RbAu(IO$_3$)$_4$, α-CsAu(IO$_3$)$_4$, and β-CsAu(IO$_3$)$_4$, the weight loss in the temperature range of 380−500 °C corresponds to the release of 1.5 I$_2$ and 4 O$_2$, 1.5 I$_2$ and 4.5 O$_2$, 1.5 I$_2$ and 4.5 O$_2$ per formula unit for RbAu(IO$_3$)$_4$, α-CsAu(IO$_3$)$_4$, and β-CsAu(IO$_3$)$_4$, respectively. The residuals at 500 °C are expected to be a mixture of RbIO$_4$ and Au or CsIO$_3$ and Au. The observed weight losses of 51.80%, 51.53%, and 52.46%, respectively, for RbAu(IO$_3$)$_4$, α-CsAu(IO$_3$)$_4$, and β-CsAu(IO$_3$)$_4$ are close to the calculated values (51.80%, 50.97%, and 50.97%). The second set of weight losses in the temperature range of 480−600 °C and the third set of weight losses (600−750, 600−810, and 600−750 °C, respectively for RbAu(IO$_3$)$_4$, α-CsAu(IO$_3$)$_4$, and β-CsAu(IO$_3$)$_4$) correspond to further decomposition of

the compounds. The total weight losses at 1000 °C are 70.65%, 81.50%, and 80.00%, respectively, for RbAu(IO$_3$)$_4$, α-CsAu(IO$_3$)$_4$, and β-CsAu(IO$_3$)$_4$, which are close to the calculated values (70.43%, 80.87%, and 80.87%) if the final residuals are assumed to be a mixture of Rb$_2$O and Au or Cs$_2$O and Au.

Optical Properties. IR spectra of α-NaAu(IO$_3$)$_4$, β-NaAu(IO$_3$)$_4$, RbAu(IO$_3$)$_4$, α-CsAu(IO$_3$)$_4$, β-CsAu(IO$_3$)$_4$, and AgAu(IO$_3$)$_4$ indicate that they are transparent in the range of 4000−900 cm^{-1} (2.5−11 μm) (Supporting Information, Figure S2). IR absorption bands in the region of 621−833 cm^{-1} are due to I−O vibrations whereas those at 505 and 528 cm^{-1} for α-NaAu(IO$_3$)$_4$, 507 and 553 cm^{-1} for β-NaAu(IO$_3$)$_4$, 501 and 523 cm^{-1} for RbAu(IO$_3$)$_4$, 487 and 517 cm^{-1} for α-CsAu(IO$_3$)$_4$, 460, 492, and 533 cm^{-1} for β-CsAu(IO$_3$)$_4$, and 502 cm^{-1} for AgAu(IO$_3$)$_4$ are the characteristic absorption bands of Au−O vibrations. These assignments are consistent with those previously reported.[6−9]

UV absorption spectra of α-NaAu(IO$_3$)$_4$, β-NaAu(IO$_3$)$_4$, RbAu(IO$_3$)$_4$, α-CsAu(IO$_3$)$_4$, β-CsAu(IO$_3$)$_4$, and AgAu(IO$_3$)$_4$ show little absorption in the range of 1000−2500 nm (1.0−2.5 μm) (Supporting Information, Figure S4). Optical diffuse reflectance spectrum studies indicate that α-NaAu(IO$_3$)$_4$, β-NaAu(IO$_3$)$_4$, RbAu(IO$_3$)$_4$, α-CsAu(IO$_3$)$_4$, β-CsAu(IO$_3$)$_4$, and AgAu(IO$_3$)$_4$ are semiconductors with optical band gaps of 2.56, 2.62, 2.53, 2.62, 2.31, and 2.40 eV, respectively (Supporting Information, Figure S5).

The solid state luminescent properties of α-NaAu(IO$_3$)$_4$, β-NaAu(IO$_3$)$_4$, RbAu(IO$_3$)$_4$, α-CsAu(IO$_3$)$_4$, β-CsAu(IO$_3$)$_4$, and AgAu(IO$_3$)$_4$ have also been investigated at room temperature under excitation at 350 nm (Figure 4). Each compound displays a strong emission band with several weak shoulder ones. The strong emission bands of α-NaAu(IO$_3$)$_4$, β-NaAu(IO$_3$)$_4$,
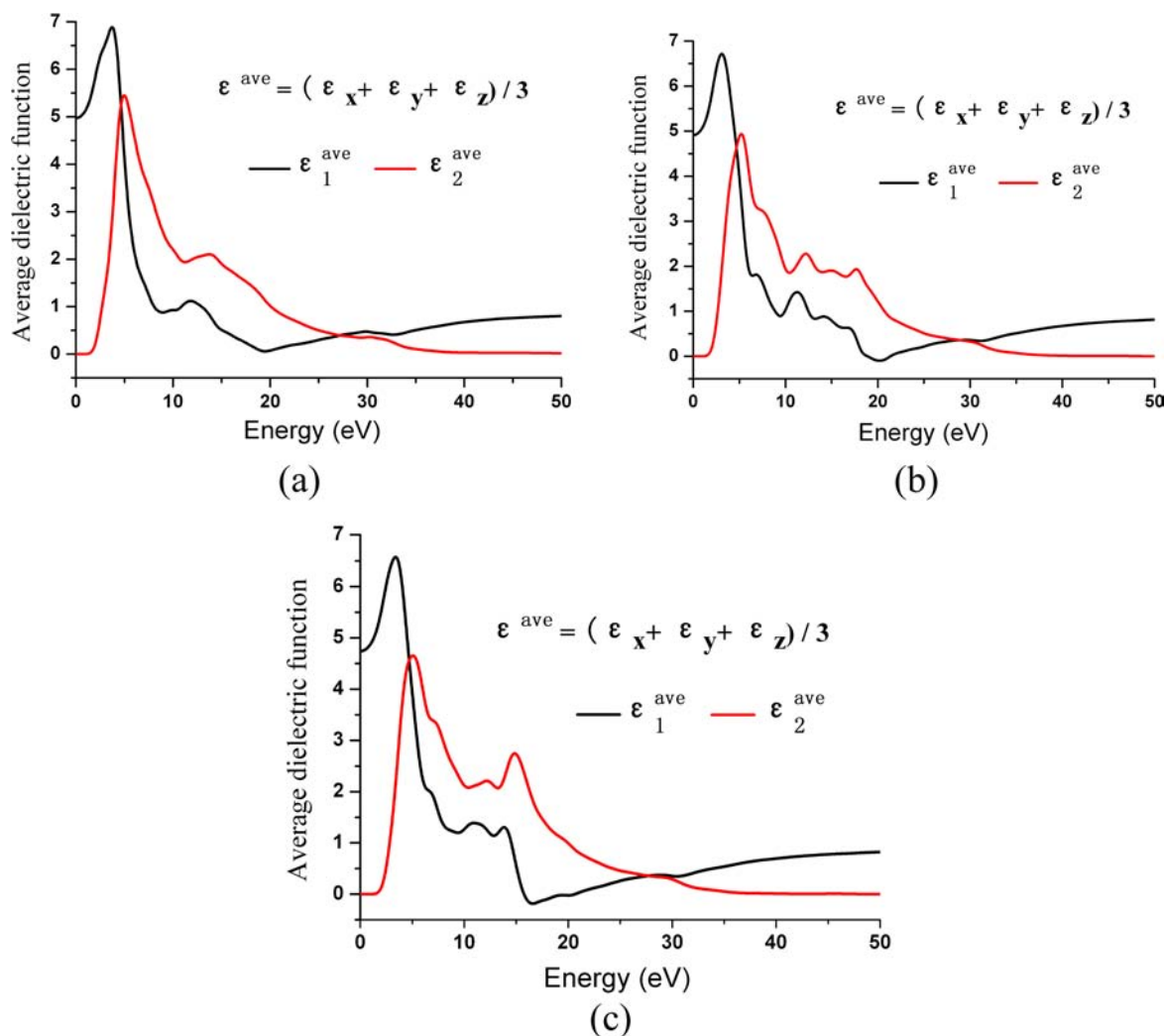
Figure 9. Calculated average imaginary part and real part of the dielectric function over three dielectric axis directions for α-NaAu(IO$_3$)$_4$ (a), RbAu(IO$_3$)$_4$ (b), and α-CsAu(IO$_3$)$_4$ (c).

RbAu(IO$_3$)$_4$, α-CsAu(IO$_3$)$_4$, β-CsAu(IO$_3$)$_4$, and AgAu(IO$_3$)$_4$ appear at 440, 415, 439, 432, 437, and 435 nm, respectively. These emission bands may be associated with Au^{3+} ions, or Ag$^+$ and Au^{3+} ions, and can be assigned to the metal-centered d→s transitions as well as the metal-anion interactions.[8d,20]

Second Harmonic Generation (SHG) Properties. Since α-NaAu(IO$_3$)$_4$, RbAu(IO$_3$)$_4$, and α-CsAu(IO$_3$)$_4$ crystallized in polar space groups, it is worth studying their SHG properties. SHG measurements on a 2.05 μm Q-switch laser with the sieved powder samples revealed that α-NaAu(IO$_3$)$_4$, RbAu(IO$_3$)$_4$, and α-CsAu(IO$_3$)$_4$ show strong SHG responses of about 1.17 ×, 1.33 ×, and 1.17 × KTP (KTiOPO$_4$), respectively. Furthermore, they are found to be type I phase-matchable (Figure 5). Based on structural data, it is expected that the strong SHG responses for the three compounds should originate from the unique arrangements of the four IO$_3$ groups in the polar Au(IO$_3$)$_4{}^-$ anion and the alignment of these polar Au(IO$_3$)$_4{}^-$ anions in their unit cells (Figures 1 and 2). It is expected that the SHG signals for RbAu(IO$_3$)$_4$ and α-CsAu(IO$_3$)$_4$ will be higher if no racemic twinning occurred. We also measured the SHG responses for these compounds on a 1.064 μm Q-switch laser with the sieved powder sample (50−70 mesh); the observed SHG responses are very weak, and the SHG signals for samples with other particle sizes are not detectable; hence

these materials are not good for applications in the UV and visible wavelength region.

Ferroelectric Properties. The ferroelectric properties of polar α-NaAu(IO$_3$)$_4$, RbAu(IO$_3$)$_4$, and α-CsAu(IO$_3$)$_4$ were investigated. These three compounds were pressed into pellets under room temperature. Ferroelectric measurements on a pellet (7.2-mm-diameter and 0.4-mm-thick) for α-NaAu(IO$_3$)$_4$, a pellet (7.2-mm-diameter and 0.42-mm-thick) for RbAu(IO$_3$)$_4$, and a pellet (7.0-mm-diameter and 0.54-mm-thick) for α-CsAu(IO$_3$)$_4$ revealed small remanent polarizations (Pr) of 0.11, 0.14, and 0.64 μC/cm^2 respectively (Supporting Information, Figure S5); hence, their ferroelectric properties are negligible. It is unlikely that the dipole moments associated with the asymmetric IO$_3$ polyhedra can be reversed, which is very unfavorable in terms of energy.[7] Thus, the polarization reversibility may be limited to the small contribution from the slightly distorted AuO$_4$ squares or derived from dielectric loss.

Theoretical Studies. To better understand the optical properties of the three polar materials, theoretical calculations based on DFT methods were made. The calculated band structures of α-NaAu(IO$_3$)$_4$, RbAu(IO$_3$)$_4$, and α-CsAu(IO$_3$)$_4$ along high symmetry points of the first Brillouin zone are plotted in Figure 6. The state energies (eV) of the lowest conduction band (L-CB) and the highest valence band (H-VB) of the three
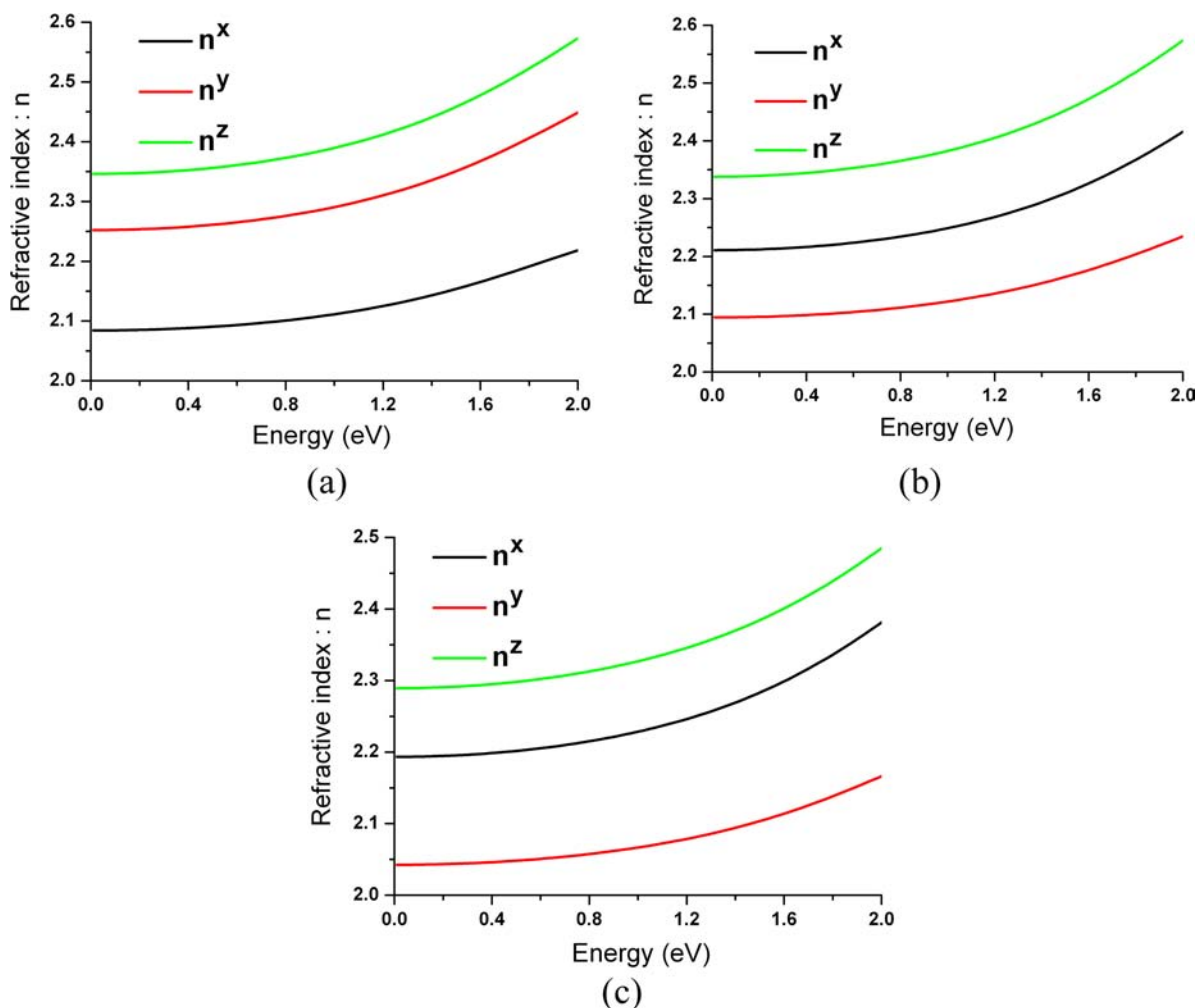
Figure 10. Calculated linear refractive indices for α-NaAu(IO$_3$)$_4$ (a), RbAu(IO$_3$)$_4$ (b), and α-CsAu(IO$_3$)$_4$ (c).

compounds are listed in Supporting Information, Table S1. The calculated band structures (Figure 6 and Supporting Information, Table S1) indicate that all three compounds are indirect band gap semiconductors with band gaps of 2.14, 2.31, and 2.30 eV for α-NaAu(IO$_3$)$_4$, RbAu(IO$_3$)$_4$, and α-CsAu(IO$_3$)$_4$, respectively. The calculated band gaps are slightly smaller than their experimental values (2.56 eV, 2.53 eV, and 2.62 eV, respectively for α-NaAu(IO$_3$)$_4$, RbAu(IO$_3$)$_4$, and α-CsAu(IO$_3$)$_4$). This is not surprising as it is well-known that the GGA does not accurately describe the eigenvalues of the electronic states, which usually causes quantitative underestimation of band gaps for semiconductors and insulators.[30] Hence, during the subsequent optical property calculations, the scissors of 0.42 eV, 0.22 eV, and 0.32 eV was adopted, respectively for α-NaAu(IO$_3$)$_4$, RbAu-(IO$_3$)$_4$, and α-CsAu(IO$_3$)$_4$).

The bands can be assigned according to the total and partial densities of states (DOS) as plotted in Figure 7. It is clear that the DOSs of three compounds are very similar to each other, so we take α-NaAu(IO$_3$)$_4$ as an example to describe them in detail. For α-NaAu(IO$_3$)$_4$ (Figure 7a), the bottom-most VBs from -50 to -47 eV originate from Na-2s states, the bands between -22.5 and -15 eV are composed of Na-2p, O-2s, and I-5s5p states, and the VBs between -11.5 and -8.0 eV arise from I-5s states mixing with a dash of O-2s2p states. We will focus on the VB and the CB in the vicinity of the Fermi level (between -8.0 and 8.0 eV), which counts for most of the bonding

characteristic in a compound. In the region of $-8.0-3.0$ eV, Au-5d states overlap fully with O-2p, and in the region of $-8.0-8.0$ eV, I-5p states overlap fully with O-2p, indicating the well-defined Au—O bonding in the AuO$_4$ planar square and I—O covalent interactions. In addition, the conduction bands from 8.0 and 20 eV are contributed by I-5s, Na-3s3p, and Au-6s6p states.

Furthermore, we also explored the linear and nonlinear optical properties of the compounds. It is noticeable that all of the optical property calculations of these compounds in this paper were based on their principal dielectric axis coordinate systems. For the determination method of the principal dielectric axes of the monoclinic crystals, please see refs 8a, 8c, and the rotation angles θ between the original coordinate axes and the principal dielectric axes in ac plane were calculated to be 29.26° and 32.85° for RbAu(IO$_3$)$_4$ and α-CsAu(IO$_3$)$_4$, respectively. For the triclinic α-NaAu(IO$_3$)$_4$ crystal, the optical permittivity tensor matrix was calculated and transformed to its diagonal form (i.e., the principal axes transformation); the obtained angles between the crystallographic axes (i.e., a, b and c) and the principal dielectric axes (i.e., x, y, and z) are listed in Table 3.

The linear optical response properties of three compounds were examined by calculating the complex dielectric function $\varepsilon(\omega) = \varepsilon_1(\omega) + i\varepsilon_2(\omega)$. Its imaginary part ($\varepsilon_2(\omega)$) can be used to describe the real transitions between the occupied and
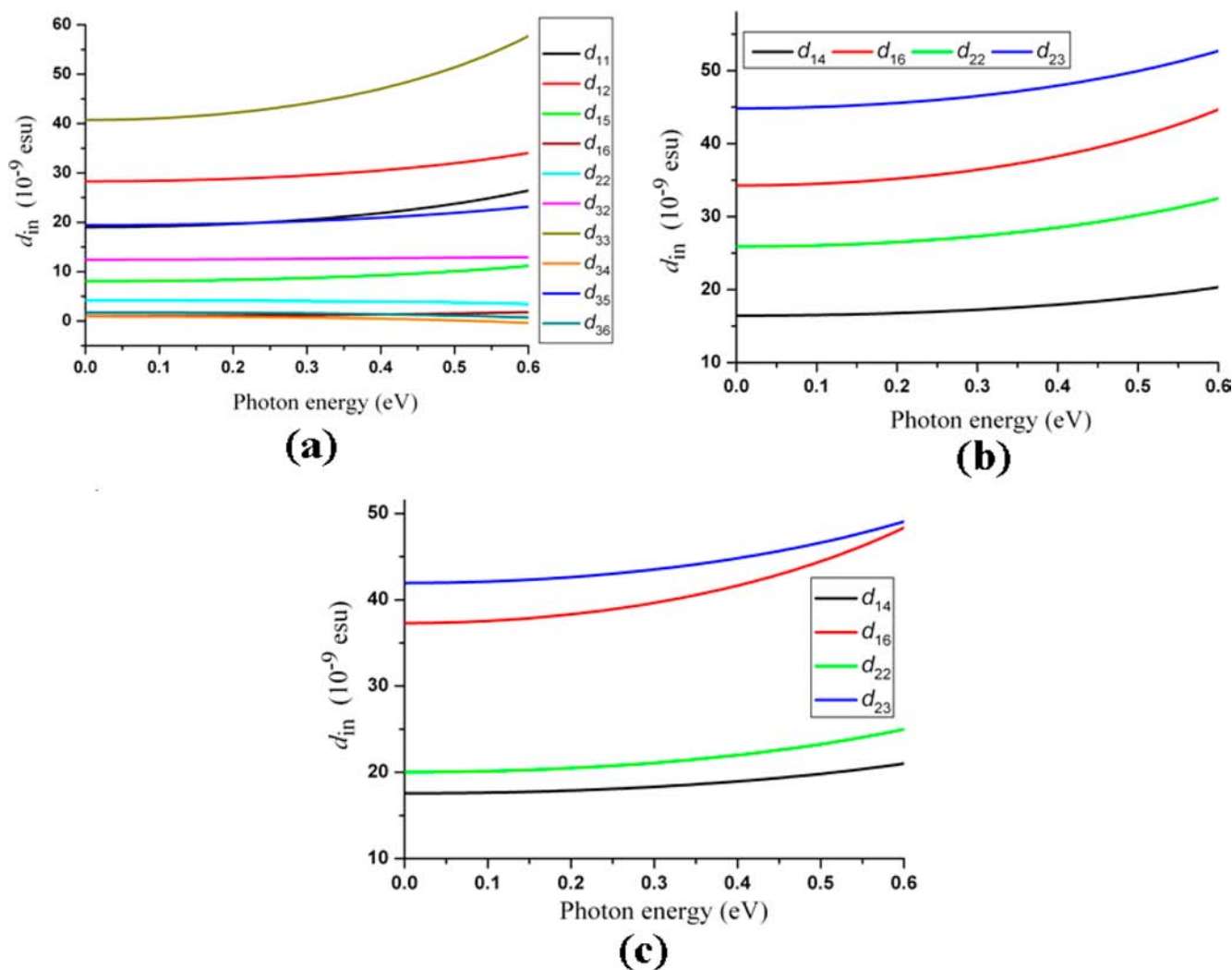
Figure 11. Calculated frequency-dependent SHG coefficients for α-NaAu(IO$_3$)$_4$ (a), RbAu(IO$_3$)$_4$ (b), and α-CsAu(IO$_3$)$_4$ (c).

unoccupied electronic states. The imaginary and real parts of the frequency-dependent dielectric functions show obvious anisotropy along the three dielectric axis directions (Figure 8). The curves of the averaged imaginary parts and real parts of the dielectric functions were obtained by $\varepsilon^{ave} = (\varepsilon_x + \varepsilon_y + \varepsilon_z)/3$ (Figure 9). The averaged imaginary parts revealed the strongest adsorption peaks of α-NaAu(IO$_3$)$_4$, RbAu(IO$_3$)$_4$, and α-CsAu(IO$_3$)$_4$ at 4.98, 5.11, and 4.98 eV, respectively, which can be mainly assigned to the electronic interband transitions from the O-2p to I-5p and Au-5d states. The average static dielectric constant $\varepsilon(0)$ of α-NaAu(IO$_3$)$_4$, RbAu(IO$_3$)$_4$, and α-CsAu(IO$_3$)$_4$ are 4.97, 4.91, and 4.74. The dispersion curves of refractive indices calculated by the formula $n^2(\omega) = \varepsilon(\omega)$ display strong anisotropy which arises from the anisotropy of the dielectric functions, $n^z > n^y > n^x$ for α-NaAu(IO$_3$)$_4$, $n^z > n^x > n^y$ for RbAu(IO$_3$)$_4$ and α-CsAu(IO$_3$)$_4$ (Figure 10). The values of n^x, n^y, and n^z at 2 μm (0.62 eV) are calculated to be 2.094, 2.266, and 2.362 for α-NaAu(IO$_3$)$_4$, 2.224, 2.104, and 2.354 for RbAu(IO$_3$)$_4$, and 2.207, 2.052, and 2.304 for α-CsAu(IO$_3$)$_4$, respectively.

Based on the space groups and the Kleinman symmetry, α-NaAu(IO$_3$)$_4$, RbAu(IO$_3$)$_4$, and α-CsAu(IO$_3$)$_4$ have 10 or 4 nonvanishing independent SHG coefficient tensors. The frequency-dependent SHG tensors of these compounds are plotted in Figure 11. At the wavelength of 2 μm (0.62 eV), the highest tensors d_{33} for α-NaAu(IO$_3$)$_4$, d_{23} for RbAu(IO$_3$)$_4$ and α-CsAu(IO$_3$)$_4$ are calculated to be 5.93 × 10^{-8}, 5.34 × 10^{-8}, and 4.96 × 10^{-8} esu, respectively. The results are slightly higher than our experimentally measured SHG responses of 1.17 ×, 1.33 ×, and 1.17 × KTP (d_{24} = 1.8 × 10^{-8} esu), as the calculations are based on single crystals that can generate much stronger SHG coefficients. Meanwhile, it is obvious that the calculated SHG coefficients of three compounds are very close to each other, which is in good agreement with the experimental results.

■ CONCLUSIONS

In summary, the introduction of the square-planar Au^{3+} cations into the monovalent metal iodate systems afforded six new mixed metal gold(III) iodates, namely, α-NaAu(IO$_3$)$_4$, β-NaAu(IO$_3$)$_4$, RbAu(IO$_3$)$_4$, α-CsAu(IO$_3$)$_4$, β-CsAu(IO$_3$)$_4$, and AgAu(IO$_3$)$_4$. More interestingly α-NaAu(IO$_3$)$_4$, RbAu(IO$_3$)$_4$, and α-CsAu(IO$_3$)$_4$ revealed moderately strong SHG responses of 1.17 ×, 1.33 ×, and 1.17 × KTP (KTiOPO$_4$), respectively, and all of them are type-I phase-matchable. Their structures are all based on Au(IO$_3$)$_4$$^-$ anions that are separated by alkali metal or silver(I) ions. When the four iodate groups in the Au(IO$_3$)$_4$$^-$ anion are located at the same side of the AuO$_4$ square plane, the Au(IO$_3$)$_4$$^-$ anion is polar, and strong SHG responses may be

11561

dx.doi.org/10.1021/ic401891f | *Inorg. Chem.* 2013, 52, 11551−11562

generated if these polar anions are aligned as in α-NaAu(IO$_3$)$_4$, RbAu(IO$_3$)$_4$, and α-CsAu(IO$_3$)$_4$. When the four iodate groups in the Au(IO$_3$)$_4^-$ anion are located at both sides of the AuO$_4$ plane, the polarrizations of these iodate groups will be canceled out and the Au(IO$_3$)$_4^-$ anion will be centrosymmetric or non-polar as in β-NaAu(IO$_3$)$_4$, β-CsAu(IO$_3$)$_4$, and AgAu(IO$_3$)$_4$. Our previous studies on the mixed metal palladium(II) iodates containing Pd(IO$_3$)$_4^-$ anions gave similar results.[9a] Both the size of the alkali metal ion and the synthetic method play important roles on the structures and SHG properties of the materials formed. Our future research efforts will be devoted to the studies of other related systems containing a MO$_4$ square planar unit.

■ ASSOCIATED CONTENT

ⓢ Supporting Information

Crystallographic data in CIF format. Further details are given in Table S1 and Figures S1−S6. This material is available free of charge via the Internet at http://pubs.acs.org.

■ AUTHOR INFORMATION

Corresponding Author
*E-mail: mjg@fjirsm.ac.cn. Fax: (+86)591-83714946.

Notes
The authors declare no competing financial interest.

■ ACKNOWLEDGMENTS

■ REFERENCES

(1) (a) Chen, C.; Liu, G. *Annu. Rev. Mater. Sci.* **1986**, *16*, 203. (b) Halasyamani, P. S.; Poeppelmeier, K. R. *Chem. Mater.* **1998**, *10*, 2753. (c) Ok, K. M.; Halasyamani, P. S. *Chem. Soc. Rev.* **2006**, *35*, 710. (d) Becker, P. *Adv. Mater.* **1998**, *10*, 979. (e) Chen, C. T.; Wang, Y. B.; Wu, B. C.; Wu, K. C.; Zeng, W. L.; Yu, L. H. *Nature* **1995**, *373*, 322.

(2) (a) Ok, K. M.; Halasyamani, P. S. *Angew. Chem., Int. Ed.* **2004**, *43*, 5489. (b) Phanon, D.; Gautier-Luneau, I. *Angew. Chem., Int. Ed.* **2007**, *46*, 8488. (c) Kim, S. H.; Yeon, J.; Halasyamani, P. S. *Chem. Mater.* **2009**, *21*, 5335. (d) Li, P. X.; Hu, C. L.; Xu, X.; Wang, R. Y.; Sun, C. F.; Mao, J. G. *Inorg. Chem.* **2010**, *49*, 4599.

(3) (a) Phanon, D.; Gautier-Luneau, I. *J. Mater. Chem.* **2007**, *17*, 1123. (b) Kong, F.; Sun, C.-F.; Yang, B.-P.; Mao, J.-G. *Struct. Bonding (Berlin)* **2012**, *144*, 43−104. (c) Sun, C. F.; Yang, B. P.; Mao, J. G. *Sci. China Chem.* **2011**, *54*, 911.

(4) (a) Lee, D. W.; Kim, S. B.; Ok, K. M. *Dalton Trans.* **2012**, *41*, 8348. (b) Ok, K. M.; Halasyamani, P. S. *Inorg. Chem.* **2005**, *44*, 9353−9359. (c) Liu, X. M.; Li, G. H.; Hu, Y. W.; Yang, M.; Kong, X. G.; Shi, Z.; Feng, S. H. *Cryst. Growth Des.* **2008**, *8*, 2453−2457.

(5) (a) Nguyen, S. D.; Yeon, J.; Kim, S. H.; Halasyamani, P. S. *J. Am. Chem. Soc.* **2011**, *133*, 12422. (b) Cao, Z.; Yue, Y.; Yao, J.; Lin, Z.; He, R.; Hu, Z. *Inorg. Chem.* **2011**, *50*, 12818−12822. (c) Sun, C.-F.; Hu, C.-L.; Mao, J.-G. *Chem. Commun.* **2012**, *48*, 4220−4222. (d) Hu, T.; Qin, L.; Kong, F.; Zhou, Y.; Mao, J. G. *Inorg. Chem.* **2009**, *48*, 2193.

(6) (a) Sykora, R. E.; Ok, K. M.; Halasyamani, P. S.; Albrecht-Schmitt, T. E. *J. Am. Chem. Soc.* **2002**, *124*, 1951. (b) Sykora, R. E.; Ok, K. M.; Halasyamani, P. S.; Wells, D. M.; Albrecht-Schmitt, T. E. *Chem. Mater.* **2002**, *14*, 2741. (c) Shehee, T. C.; Sykora, R. E.; Ok, K. M.; Halasyamani, P. S.; Albrecht-Schmitt, T. E. *Inorg. Chem.* **2003**, *42*, 457.

(7) (a) Chang, H. Y.; Kim, S. H.; Halasyamani, P. S.; Ok, K. M. *J. Am. Chem. Soc.* **2009**, *131*, 2426. (b) Chang, H. Y.; Kim, S. H.; Ok, K. M.; Halasyamani, P. S. *J. Am. Chem. Soc.* **2009**, *131*, 6865.

(8) (a) Sun, C. F.; Hu, C. L.; Xu, X.; Ling, J. B.; Hu, T.; Kong, F.; Long, X. F.; Mao, J. G. *J. Am. Chem. Soc.* **2009**, *131*, 9486. (b) Sun, C. F.; Hu, C. L.; Xu, X.; Yang, B. P.; Mao, J. G. *J. Am. Chem. Soc.* **2011**, *133*, 5561. (c) Yang, B. P.; Hu, C. L.; Xu, X.; Sun, C. F.; Zhang, J. H.; Mao, J. G. *Chem. Mater.* **2010**, *22*, 1545. (d) Sun, C.-F.; Hu, T.; Xu, X.; Mao, J.-G. *Dalton Trans.* **2010**, *39*, 7960−7967. (e) Suffren, Y.; Gautier-Luneau, I. *Eur. J. Inorg. Chem.* **2012**, 4264−4267. (f) Yang, B.-P.; Hu, C.-L.; Xu, X.; Huang, C.; Mao, J.-G. *Inorg. Chem.* **2013**, *52*, 5378−5384. (g) Huang, C.; Hu, C.-L.; Xu, X.; Yang, B.-P.; Mao, J.-G. *Dalton Trans.* **2013**, *42*, 7051−7058.

(9) (a) Sun, C.-F.; Hu, C.-L.; Xu, X.; Mao, J.-G. *Inorg. Chem.* **2010**, *49*, 9581−9589. (b) Ling, J.; Albrecht-Schmitt, T. E. *Eur. J. Inorg. Chem.* **2007**, *5*, 652. (c) Dengel, A. C.; Elhendawy, A. M.; Griffith, W. P.; Mostafa, S. I.; Williams, D. J. *Dalton Trans.* **1992**, 3489. (d) Hector, A. L.; Levason, W.; Webster, M. *Inorg. Chim. Acta* **2003**, *343*, 90.

(10) Wendlandt, W. M.; Hecht, H. G. *Reflectance Spectroscopy*; Interscience: New York, 1966.

(11) Kurtz, S. W.; Perry, T. T. *J. Appl. Phys.* **1968**, *39*, 3798.

(12) Sheldrick, G. M. *SHELXTL, Crystallographic Software Package, SHELXTL*, Version 5.1; Bruker-AXS: Madison, WI, 1998.

(13) (a) Segall, M. D.; Lindan, P. J. D.; Probert, M. J.; Pickard, C. J.; Hasnip, P. J.; Clark, S. J.; Payne, M. C. *J. Phys.: Condens. Matter* **2002**, *14*, 2717. (b) Milman, V.; Winkler, B.; White, J. A.; Pickard, C. J.; Payne, M. C.; Akhmatskaya, E. V.; Nobes, R. H. *Int. J. Quantum Chem.* **2000**, *77*, 895.

(14) Perdew, J. P.; Burke, K.; Ernzerhof, M. *Phys. Rev. Lett.* **1996**, *77*, 3865.

(15) Lin, J. S.; Qteish, A.; Payne, M. C.; Heine, V. *Phys. Rev. B* **1993**, *47*, 4174.

(16) Bassani, F.; Parravicini, G. P. *Electronic States and Optical Transitions In Solids*; Pergamon Press Ltd.: Oxford, U.K., 1975; Vol. 149.

(17) (a) Ghahramani, E.; Moss, D. J.; Sipe, J. E. *Phys. Rev. B* **1991**, *43*, 8990. (b) Ghahramani, E.; Moss, D. J.; Sipe, J. E. *Phys. Rev. Lett.* **1990**, *64*, 2815.

(18) (a) Duan, C. G.; Li, J.; Gu, Z. Q.; Wang, D. S. *Phys. Rev. B* **1999**, *60*, 9435. (b) Guo, G. Y.; Chu, K. C.; Wang, D. S.; Duan, C. G. *Phys. Rev. B* **2004**, *69*, 205416. (c) Guo, G. Y.; Lin, J. C. *Phys. Rev. B* **2005**, *72*, 075416. (d) Guo, G. Y.; Lin, J. C. *Phys. Rev. B* **2008**, *77*, 049901.

(19) Geb, J.; Jansen, M. *J. Solid State Chem.* **1996**, *122*, 364−370.

(20) (a) Ford, P. C.; Vogler, A. *Acc. Chem. Res.* **1993**, *26*, 220. (b) Che, C. M.; Tse, M. C.; Chan, M. C. W.; Cheung, K. K.; Phillips, D. L.; Leung, K. H. *J. Am. Chem. Soc.* **2000**, *122*, 2464. (c) Henary, M.; Zink, J. I. *Inorg. Chem.* **1991**, *30*, 3111. (d) Sabin, F.; Ryu, C. K.; Ford, P. C.; Vogler, A. *Inorg. Chem.* **1992**, *31*, 1941.